CSMA 2026
17ème Colloque National en Calcul des Structures
18-22 Mai 2026, Presqu'île de Giens (Var)

Investigation of size effects in miniaturized components with free edges using an FFT-based solver for non-local crystal plasticity

Lei CAI[1], François BIGNONNET [1], Laurent STAINIER [1]

[1] *Nantes Université, École Centrale Nantes, CNRS, GeM, UMR 6183, F-44000 Nantes, France*
{lei.cai, laurent.stainier}@ec-nantes.fr, francois.bignonnet@univ-nantes.fr

Résumé — This work presents a numerical investigation of size effects in miniaturized components using a Gurtin-type non-local crystal plasticity model. Simulations are performed using an efficient FFT-based implementation, with an adaptive Barzilai-Borwein non-linear gradient descent solver. Size effects are systematically investigated using pseudo two-dimensional RVEs with free edge boundary conditions. The non-local model successfully captures intrinsic size effects, with enhanced flow stress as the average crystal size decreases, which is attributed to the non-local energetic backstress.

Mots clés — strain gradient plasticity, size effects, fast Fourier transform (FFT) , free edges.

1 Introduction

Over the past few decades, significant developments in micro-electronics have led to a dramatically increasing demand for miniaturized products. When geometrical dimensions down-scale from macroscopic to microscopic level, material behaviors become no longer size-independent, rendering conventional forming process rules inapplicable. Experimental observations reveal pronounced size effects at small scales, where strain gradients and dislocation interactions become significant [1, 2]. Classical continuum plasticity theories, lacking intrinsic length scales, are inadequate for capturing these size-dependent phenomena in miniaturized components.

Strain gradient plasticity theories have emerged as a robust framework to address size-dependent plasticity by introducing internal length scales into the constitutive description [3, 4]. Among various formulations, the Gurtin-type non-local crystal plasticity model [5] provides an elegant framework, where energetic backstresses arise naturally from the gradient of plastic slip. In this work, the Gurtin-type strain gradient crystal plasticity model formulated under the small deformation regime will be employed.

The Fast Fourier Transform (FFT)-based spectral method [6] has emerged as a highly efficient alternative to finite element methods for computing the mechanical response of periodic polycrystalline materials. Early FFT implementations for crystal plasticity adopted local constitutive formulations, rendering predictions size-independent. Recent developments [7, 8] have successfully extended FFT methods to incorporate strain gradient effects, enabling efficient treatment of non-local crystal plasticity. In this work, we employ the FFT-based spectral method combined with an adaptive Barzilai-Borwein gradient descent solver [9] to implement the Gurtin-type non-local crystal plasticity model.

The paper is organized as follows : Section 2 presents the non-local crystal plasticity formulation, Section 3 describes the FFT-based numerical implementation, Section 4 investigates size effects, and Section 5 presents concluding remarks.

2 Non-local crystal plasticity formulation

In this work, the Gurtin [5] type non-local crystal plasticity model under small deformation framework is employed and is briefly summarized.

2.1 Kinematics

In the framework of small deformation, the displacement gradient $\nabla\mathbf{u}$ can be additively split into elastic and plastic parts :

$$\nabla\mathbf{u} = \mathbf{H}_e + \mathbf{H}_p \tag{1}$$

where $\mathbf{H}_e$ and $\mathbf{H}_p$ represent respectively the elastic distortion, due to stretch and rotation of the underlying lattice, and the plastic distortion. Their symmetric parts define the elastic and plastic strain tensors :

$$\varepsilon_e = \frac{1}{2}\left[\mathbf{H}_e + \mathbf{H}_e^T\right],\ \varepsilon_p = \frac{1}{2}\left[\mathbf{H}_p + \mathbf{H}_p^T\right] \tag{2}$$

In single-crystal plasticity framework, it is widely acknowledged that plastic flow occurs through slip on prescribed slip systems, with each system α defined by a slip direction $\mathbf{s}^\alpha$ and a slip-plane normal $\mathbf{m}^\alpha$ unit vectors. With this description of plastic flow, the rate of plastic distortion $\mathbf{H}_p$ can be expressed as :

$$\dot{\mathbf{H}}_p = \sum_{\alpha=1}^{q} \dot{\gamma}^\alpha \left[\mathbf{s}^\alpha \otimes \mathbf{m}^\alpha\right] \tag{3}$$

where $\dot{\gamma}^\alpha$ is the rate of plastic slip on slip system α, q is the total number of slip systems, and "$\otimes$" is the tensor product operator.

Using this expression, the plastic strain rate tensor $\dot{\varepsilon}_p$ can be written as :

$$\dot{\varepsilon}_p = \sum_{\alpha=1}^{q} \dot{\gamma}^\alpha \mathbf{P}^\alpha,\ \ \mathbf{P}^\alpha = \frac{1}{2}\left(\mathbf{s}^\alpha \otimes \mathbf{m}^\alpha + \mathbf{m}^\alpha \otimes \mathbf{s}^\alpha\right). \tag{4}$$

A key feature of the Gurtin [5] formulation is the incorporation of the Nye tensor (also termed the geometric dislocation density tensor) directly into the constitutive framework. This tensor, defined as the curl of the plastic distortion, provides a measure of the geometrically necessary dislocation content :

$$\mathbf{G} = \operatorname{curl}\mathbf{H}_p \tag{5}$$

This fundamental kinematic quantity serves as the basis for introducing non-local effects through an energetic contribution to the free energy, as detailed in the subsequent sections.

2.2 Force balances

The balance equations are derived based on a generalization of the virtual power density of internal forces. Detailed derivations can be found in [10, 5]. For the static case, the macroscopic balance equations and the associated traction conditions read :

$$\left\{\begin{array}{rcll} \nabla\cdot\boldsymbol{\sigma} & = & \mathbf{0} & \text{in } \mathscr{V} \\ \boldsymbol{\sigma}\cdot\mathbf{n} & = & \mathbf{t} & \text{on } \mathscr{S} \end{array}\right. \tag{6}$$

where $\mathbf{n}$ denotes the outward unit normal to $\mathscr{S}$. Similarly, the microscopic balance equation and the associated traction condition on each slip system α are given by :

$$\left\{\begin{array}{rcll} \tau^\alpha + \nabla\cdot\xi^\alpha - \pi^\alpha & = & 0 & \text{in } \mathscr{V} \\ \xi^\alpha\cdot\mathbf{n} & = & \chi^\alpha & \text{on } \mathscr{S} \end{array}\right. \tag{7}$$

Here, σ denotes the macroscopic stress tensor, $\tau^\alpha = \sigma : (\mathbf{s}^\alpha \otimes \mathbf{m}^\alpha)$ is the resolved shear stress on slip system α, π^α is the microscopic stress scalar work-conjugate to γ^α, and ξ^α is the microscopic stress vector work-conjugate to $\nabla\gamma^\alpha$.

2.3 Constitutive laws

2.3.1 Energetic constitutive laws

The energetic processes are represented by the total free energy density ψ, which consists of two contributions : an elastic part ψ_e and a non-local energetic part ψ_G associated with the geometric dislocation density tensor. The total free energy can be written as :

$$\psi = \psi_e(\varepsilon_e) + \psi_G(\mathbf{G}) \tag{8}$$

The elastic part ψ_e is assumed to be a quadratic function of the elastic strain $\boldsymbol{\varepsilon}_e$ as $\psi_e(\boldsymbol{\varepsilon}_e) = \frac{1}{2}\boldsymbol{\varepsilon}_e : \mathbf{C} : \boldsymbol{\varepsilon}_e$, from which the (energetic) macroscopic stress tensor $\boldsymbol{\sigma}$ is derived as $\boldsymbol{\sigma} = \mathbf{C} : \boldsymbol{\varepsilon}_e$. The $\mathbf{C}$ is the elastic stiffness tensor, which is assumed to be symmetric and positive-definite.

The non-local energetic contribution ψ_G, associated with the geometric dislocation density tensor, is assumed to be a quadratic function following [5] :

$$\psi_G = \frac{1}{2} X_0 l_{\text{en}}^2 |\mathbf{G}|^2 \tag{9}$$

where X_0 is a constant representing the energetic slip resistance, and l_{en} is the energetic length scale. It should be noted that the quadratic form is employed here as a pragmatic choice, since the most appropriate form of defect energy remains an open question in the literature [11]. Alternative non-quadratic formulations have been investigated [10, 12], revealing that the choice of defect energy form can lead to complex nonlinear hardening effects associated with non-locality, particularly under non-proportional loading conditions.

For the quadratic form adopted here, the energetic microscopic stress vector ξ^{α}_{en} on slip system α is derived as :

$$\xi^{\alpha}_{en} = \frac{\partial \psi_G}{\partial \nabla \gamma^{\alpha}} = \sum_{\beta} \left[\mathbf{M}^{\alpha\beta} \nabla \gamma^{\beta} \right] \tag{10}$$

where the modulus tensor $\mathbf{M}^{\alpha\beta}$ is defined as :

$$\mathbf{M}^{\alpha\beta} = X_0 l_{\text{en}}^2 \left(\mathbf{s}^{\beta} \cdot \mathbf{s}^{\alpha} \right) \left(\left(\mathbf{m}^{\alpha} \cdot \mathbf{m}^{\beta} \right) \mathbf{I} - \left(\mathbf{m}^{\alpha} \otimes \mathbf{m}^{\beta} \right) \right) \tag{11}$$

2.3.2 Dissipative constitutive laws

Following the Gurtin formulation, dissipative effects are assumed to contribute only to the lower-order microscopic stress π^{α}, while the higher-order microscopic stress ξ^{α} is purely energetic (i.e., $\pi^{\alpha} = \pi^{\alpha}_{dis}$ and $\xi^{\alpha} = \xi^{\alpha}_{en}$). The dissipative microscopic stress follows a viscoplastic power-law relation :

$$\pi^{\alpha} = S^{\alpha}_{\pi} \left[\frac{\dot{\gamma}^{\alpha}}{\dot{\gamma}^{\alpha}_0} \right]^m \frac{\dot{\gamma}^{\alpha}}{|\dot{\gamma}^{\alpha}|} \tag{12}$$

where S^{α}_{π} is the dissipative slip resistance, $\dot{\gamma}^{\alpha}_0$ is the reference slip rate, and m is the rate-sensitivity parameter. The evolution of the dissipative slip resistance is given by :

$$\dot{S}^{\alpha}_{\pi} = \sum_{\beta=1}^{q} h^{\alpha\beta}_{\pi} \left| \dot{\gamma}^{\beta} \right| \quad \text{with} \quad S^{\alpha}_{\pi}(0) = S_{\pi 0} > 0$$

where $h^{\alpha\beta}_{\pi}$ is the hardening modulus and $S_{\pi 0}$ is the initial dissipative slip resistance.

2.4 Flow rule

Substituting the constitutive expressions into (7) and re-arranging, the flow rule for each slip system α can be written as :

$$\tau^{\alpha} = \underbrace{-\nabla \cdot \xi^{\alpha}_{en}}_{\tau^{\alpha}_b} + \pi^{\alpha}_{dis}. \tag{13}$$

The first term on the right-hand τ^{α}_b represents the energetic backstress. The flow rule clearly shows that the resolved shear stress τ^{α} is balanced by the energetic backstress τ^{α}_b and the dissipative hardening.

3 Numerical implementation

The constitutive equations derived in Section 2 are solved numerically using the Fast Fourier Transform (FFT) method. The computational framework is summarized in Algorithm 1, which evolves the state variables from time t to $t + \Delta t$ (as detailed in the Input and Output sections of the algorithm). Note

Algorithm 1 Pseudo code of the FFT-based implementation of non-local crystal plasticity model

Starting at time step t with inputs, we advance to $t+\Delta t$ with outputs.

Input : $\left\{\sigma_t, \varepsilon_t, \mathrm{iv}_t\left(\gamma_t^\alpha, \pi_t^\alpha, \tau_{b,t}^\alpha\right), \Delta t\right\} \rightarrow$ **Output** : $\left\{\sigma, \varepsilon, \mathrm{iv}\left(\gamma^\alpha, \pi^\alpha, \tau_b^\alpha\right)\right\}$

Step1 : initialization

— Strain extrapolation[6] : $\varepsilon^{(0)} = f\left(\varepsilon_t, \varepsilon_{t-1}, t-\Delta t, t, t+\Delta t\right)$

— Constitutive integration

$$\left\{\sigma^{(0)}, \mathrm{iv}^{(0)}\left(\gamma^{\alpha(0)}, \pi^{\alpha(0)}, \tau_{b,t}^\alpha\right)\right\} = \mathrm{umat}\left(\varepsilon^{(0)}, \sigma_t, \varepsilon_t, \mathrm{iv}_t\left(\gamma_t^\alpha, \pi_t^\alpha, \tau_{b,t}^\alpha\right)\right)$$

Step2 : Barzilai-Borwein iterative solver

— Compute residual : $\mathbf{r}^{(i)} = \Gamma_0 : \sigma^{(i)}$, $\beta^{(i)} = \mathbf{r}^{(i-1)} \cdot \sigma^{(i)}$

— Update step size : $s^{(i)} = s^{(i-1)} / (1 - \beta^{(i)} / \left\|\mathbf{r}^{(i-1)}\right\|_{L^2}^2)$

— Update strain : $\varepsilon^{(i+1)} = \varepsilon^{(i)} - s^{(i)} \mathbf{r}^{(i)}$

— Constitutive integration

$$\left\{\sigma^{(i+1)}, \mathrm{iv}^{(i+1)}\left(\gamma^{\alpha(i+1)}, \pi^{\alpha(i+1)}, \tau_{b,t}^\alpha\right)\right\} = \mathrm{umat}\left(\varepsilon^{(i+1)}, \sigma_t, \varepsilon_t, \mathrm{iv}^{(i)}\left(\gamma^{\alpha(i)}, \pi^{\alpha(i)}, \tau_{b,t}^\alpha\right), \Delta t\right)$$

— Check convergence : if err $= \left\|\mathbf{r}^{(i)}\right\|_{L^2} / \|\bar{\sigma}^{(i)}\| <$ tol then exit, repeat if not converged

Step 3 : update higher-order stress :

— Gradient in Fourier space :

$$\hat{\gamma}^\alpha = \mathrm{FT}\left(\gamma^\alpha\right), \nabla\hat{\gamma}^\alpha = \mathrm{grad\_op}\left\{\hat{\gamma}^\alpha\right\}$$

— Higher-order stress in real space

$$\nabla\gamma^\alpha = \mathrm{FT}^{-1}\left(\nabla\hat{\gamma}^\alpha\right), \xi^\alpha = \sum_\beta \left[\mathbf{M}^{\alpha\beta} \nabla\gamma^\beta\right]$$

— Backstress in Fourier space :

$$\hat{\xi}^\alpha = \mathrm{FT}\left(\xi^\alpha\right), \hat{\tau}_b^\alpha = \mathrm{div\_op}\left\{\hat{\xi}^\alpha\right\}$$

— Backstress in real space

$$\tau_b^\alpha = FT^{-1}\left(\hat{\tau}_b^\alpha\right)$$

that here **iv** denotes a collection of internal variables for implementation convenience and all variables without subscripts are evaluated at time $t+\Delta t$ unless stated explicitly. In the initialization stage, strain extrapolation is employed [6], and the state variables are integrated using a fully implicit method via a UMAT-like function [13]. Then, the initialized state variables are sent to the Barzilai-Borwein solver [9] for iterative loop until convergence on the macroscopic force balance in (6) is achieved. It should be noted that the backstress is always treated as constant, using that in time t. Finally, the non-local stress is updated with converged outputs from the Barzilai-Borwein solver. This manner of updating backstress is the so-called explicit update type as [7, 8, 14].

For spatial discretization, the periodic microstructure with volume $V = L_1 \times L_2 \times L_3$ is represented on a regular voxel grid of $N_1 \times N_2 \times N_3$ points. The divergence, gradient, and Green operator Γ_0 are discretized using first-order finite differences, as proposed in [15]. As a result, the divergence and gradient operators, which are here applied in the Fourier space, could alternatively be evaluated in the direct space (see Algorithm 1, step 3). The implementation of the overall relies on a Julia FFT library developed at the GeM laboratory referred to previous work of [16].

t/d	Number of grains	RVE size (voxels)	Grain size d (μm)	Total voxels
2	4	$24 \times 24 \times 1$	0.5	576
3	9	$36 \times 36 \times 1$	0.333	1296
4	16	$48 \times 48 \times 1$	0.25	2304
5	25	$60 \times 60 \times 1$	0.2	3600
6	36	$72 \times 72 \times 1$	0.167	5184
7	49	$84 \times 84 \times 1$	0.143	7056
8	64	$96 \times 96 \times 1$	0.125	9216

TABLE 1 – RVE configurations with varying thickness-to-grain-size ratios.

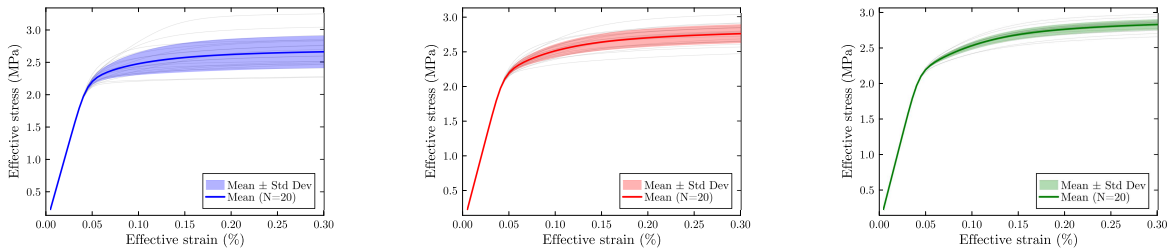

(a) t/d=2 (b) t/d=4 (c) t/d=8

FIGURE 1 – Extrinsic size effects : averaged stress-strain curves with statistical dispersion bands for different thickness-to-grain-size ratios : (a) $t/d = 2$, (b) $t/d = 4$, (c) $t/d = 8$. The shaded regions represent statistical variability over multiple orientation realizations.

4 Results

4.1 Investigation of size effects with free edge setup in RVE

To investigate the size-dependent plastic behavior, a series of pseudo two-dimensional representative volume elements (RVEs) are generated using Neper [17]. Following the approach of Gelebart [18], the free edge condition is implemented by applying periodicity in the X- and Z-directions while adding one additional layer of voxels with near-zero elastic stiffness (10^{-12} times of the material elasticity adopted for numerical convergence of CP constitutive integration) on the $+Y$-face to relax the periodic boundary condition. Table 1 summarizes the RVE configurations with varying thickness-to-grain-size ratios investigated in this study. Each grain contains 12×12 voxels in average to ensure sufficient spatial resolution. The material parameters are chosen the same as [7].

4.1.1 Extrinsic size effects

Figure 1 presents the stress-strain responses averaged over 20 random realizations of the orientations for three representative RVE configurations with different thickness to grain-size ratios, under macroscopic uniaxial traction in the X-direction. The thickness of the sample in the Y-direction is set to $t = 1\mu m$, while the average grain size d is varied according to Table 1. These results illustrate extrinsic size effects, characterized by the decrease in average in flow stress as the number of grains across the specimen thickness decreases. To further quantify the extrinsic size effect, Figure 2a directly compares the averaged stress-strain curves across different t/d ratios. The systematic increase in flow stress with increasing t/d (e.g., $t/d = 2,3,4$) demonstrates the "smaller is stronger" trend.

However, when t/d is larger than 5 as shown in Figure 2a, the stress-strain curves seem to converge to a certain level. This prediction contradicts experimental observations reported in the literature (see experimental evidence from [19]), where continued increase in t/d ratio consistently leads to enhanced flow stress. This discrepancy highlights the inadequacy of classical crystal plasticity models in accurately capturing the "smaller is stronger" phenomenon induced by non-local effects. The lack of an intrinsic length scale in conventional crystal plasticity (CCP) models prevents them from properly accounting for

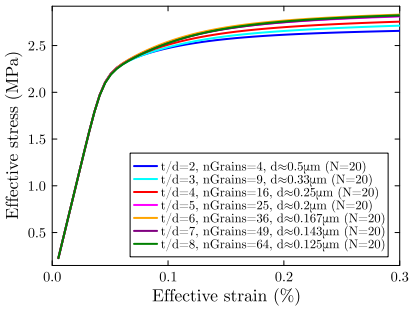

(a) Extrinsic size effects ($l_{en} = 0$)

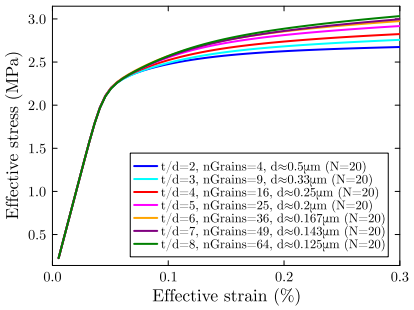

(b) Intrinsic size effects ($l_{en} = 0.2\mu m$)

FIGURE 2 – Averaged stress-strain responses for different t/d ratios : extrinsic of local CP v.s. intrinsic size effects of non-local.

gradient-dependent hardening mechanisms. To address this limitation, we next investigate intrinsic size effects arising from the non-local energetic length scale in the following section.

4.1.2 Intrinsic size effects

In contrast to the extrinsic size effects observed in the previous section, intrinsic size effects arise from the internal length scale l_{en} embedded in the non-local constitutive model. Figure 2b presents the averaged stress-strain curves for a fixed energetic length scale of $l_{\text{en}} = 0.2\mu m$ with varying grain sizes. The results clearly demonstrate that increasing the l_{en}/d ratio leads to enhanced flow stress, confirming the strengthening effect of non-local interactions.

To further elucidate the underlying mechanisms, Figure 3 presents the spatial distribution of the energetic backstress τ_b for different t/d ratios at a fixed internal length scale ($l_{\text{en}} = 0.2\mu m$) and applied strain of 0.3%. The contour plots reveal distinct patterns of backstress accumulation at grain boundaries that correlate with the observed size effects. A key observation is that larger t/d ratios exhibit significantly higher backstress peak values, which constitutes the primary contribution to the enhanced flow stress. This trend of increasing backstress magnitude with larger l_{en}/d ratios is in accordance with experimental investigations reported by [20].

5 Conclusion

This work presented an efficient FFT-based implementation of the Gurtin-type non-local crystal plasticity model to investigate size-dependent mechanical behavior in miniaturized components. The adaptive Barzilai-Borwein gradient descent scheme is adopted to accelerate convergence compared to the standard Moulinec-Suquet scheme.

Size effects were systematically investigated using pseudo two-dimensional RVEs with free edge boundary conditions. Classical crystal plasticity models exhibit a "smaller is stronger" trend but the flow stress converges at higher t/d ratios, highlighting the limitations of local formulations. The non-local model successfully captures intrinsic size effects, where enhanced flow stress arises from energetic backstress peaks that increase with t/d ratios, consistent with experimental observations [20].

Future work will focus on extending the framework to simulate thin metal sheets with Physical Vapor Deposition (PVD) coatings as reported by [21], where the interplay between coating properties and substrate microstructure introduces additional complexities in size-dependent behavior.

Acknowledgements

This work has been funded, in whole or in part, by l'Agence Nationale de la Recherche (ANR), project ANR-23-CE08-0036 (MOCAMOR).

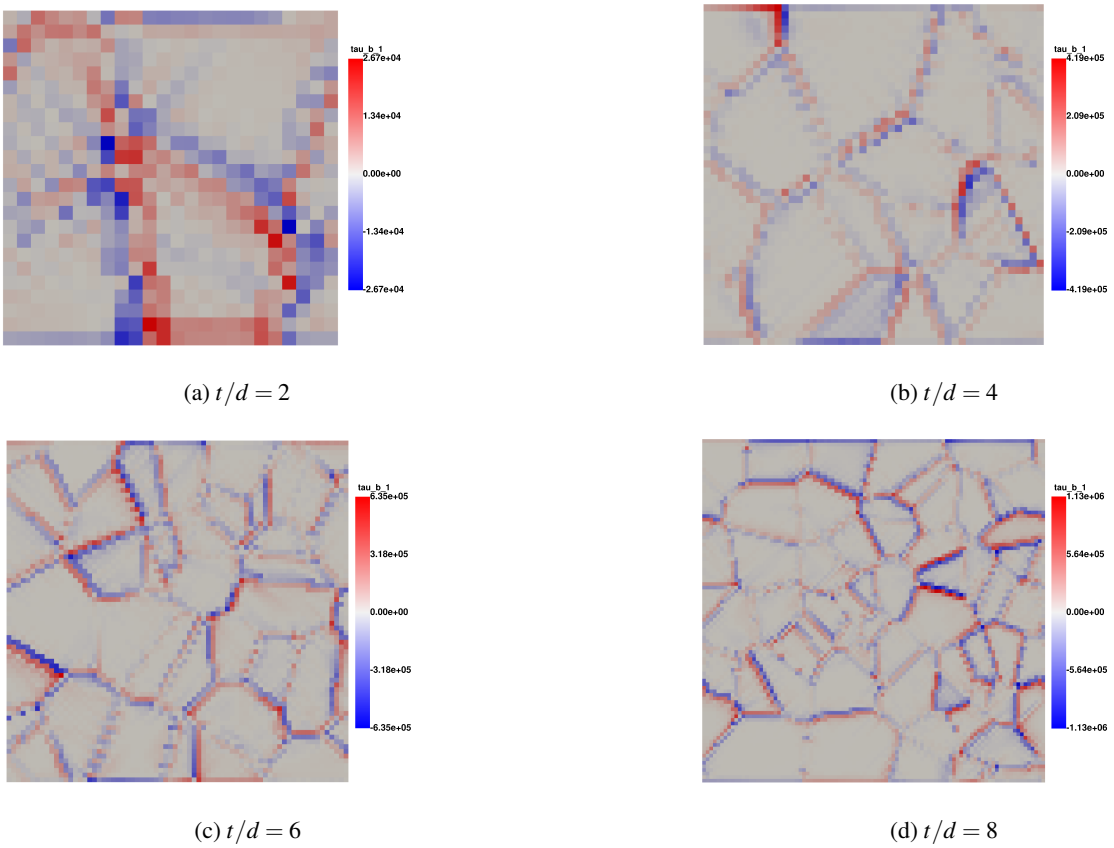

(a) $t/d = 2$ (b) $t/d = 4$

(c) $t/d = 6$ (d) $t/d = 8$

FIGURE 3 – Spatial distribution of energetic backstress τ_b (in Pa) for different t/d ratios at fixed $l_{\text{en}} = 0.2\mu m$ and 0.3% applied strain.

Références

[1] N. A. Fleck, G. M. Muller, M. F. Ashby, and J. W. Hutchinson. Strain gradient plasticity : Theory and experiment. *Acta Metallurgica Et Materialia*, 42(2) :475–487, 1994.

[2] W. D. Nix and H. Gao. Indentation size effects in crystalline materials : A law for strain gradient plasticity. *Journal of the Mechanics and Physics of Solids*, 46(3) :411–425, 1998.

[3] N. A. Fleck and J. W. Hutchinson. Strain Gradient Plasticity. *Advances in Applied Mechanics*, 33(C) :295–361, 1997.

[4] P. Gudmundson. A unified treatment of strain gradient plasticity. *Journal of the Mechanics and Physics of Solids*, 52(6) :1379–1406, 2004.

[5] M. E. Gurtin. A gradient theory of single-crystal viscoplasticity that accounts for geometrically necessary dislocations. *Journal of the Mechanics and Physics of Solids*, 50(1) :5–32, 2002.

[6] H. Moulinec and P. Suquet. A numerical method for computing the overall response of nonlinear composites with complex microstructure. *Computer Methods in Applied Mechanics and Engineering*, 157(1–2) :69–94, 1998.

[7] R. A. Lebensohn and A. Needleman. Numerical implementation of non-local polycrystal plasticity using fast Fourier transforms. *Journal of the Mechanics and Physics of Solids*, 97 :333–351, 2016.

[8] A. Lame Jouybari, S. El Shawish, and L. Cizelj. Fast Fourier transform approach to Strain Gradient Crystal Plasticity : Regularization of strain localization and size effect. *International Journal of Plasticity*, 183 :104153, 2024.

[9] M. Schneider. On the Barzilai-Borwein basic scheme in FFT-based computational homogenization. *International Journal for Numerical Methods in Engineering*, 118(8) :482–494, 2019.

[10] L. Cai. *Plasticité cristalline à gradients dans un cadre de grandes déformations pour modéliser les effets de taille dans les composants miniaturisés : Application à la localisation des déformations dans les tôles métalliques monocristallines et polycristallines*. PhD thesis, HESAM Université, 2021.

[11] M. E. Gurtin, L. Anand, and S. P. Lele. Gradient single-crystal plasticity with free energy dependent on dislocation densities. *Journal of the Mechanics and Physics of Solids*, 55(9) :1853–1878, 2007.

[12] M. Jebahi, L. Cai, and F. Abed-Meraim. Strain gradient crystal plasticity model based on generalized non-quadratic defect energy and uncoupled dissipation. *International Journal of Plasticity*, 126 :102617, 2020.

[13] Y. Huang. A user-material subroutine incorporating single crystal plasticity in the abaqus finite element program. *Division of Applied Sciences, Harvard University*, page 47, 1991.

[14] A. Marano, G. Lionel, L. Gélébart, and S. Forest. FFT-based simulations of slip and kink bands formation in 3D polycrystals : Influence of strain gradient crystal plasticity. *Journal of the Mechanics and Physics of Solids*, page 104295, 2021.

[15] F. Willot. Fourier-based schemes for computing the mechanical response of composites with accurate local fields. *Comptes Rendus Mécanique*, 343(3) :232–245, 2015.

[16] F. Bignonnet. *Caractérisation expérimentale et modélisation micro-mécanique de la perméabilité et la résistance de roches argileuses*. PhD thesis, Université Paris-Est, 2014.

[17] R. Quey, P. R. Dawson, and F. Barbe. Large-scale 3d random polycrystals for the finite element method : Generation, meshing and remeshing. *Computer Methods in Applied Mechanics and Engineering*, 200(17-20) :1729–1745, 2011.

[18] L. Gélébart. Grain size effects and weakest link theory in 3D crystal plasticity simulations of polycrystals. *Comptes Rendus. Physique*, 22(S3) :313–330, 2021.

[19] C. Keller, E. Hug, A. M. Habraken, and L. Duchêne. Effect of stress path on the miniaturization size effect for nickel polycrystals. *International Journal of Plasticity*, 64 :26–39, 2015.

[20] C. Keller, E. Hug, and D. Chateigner. On the origin of the stress decrease for nickel polycrystals with few grains across the thickness. *Materials Science and Engineering : A*, 500(1–2) :207–215, 2009.

[21] P.-A. Dubos, A. Zaouali, P.-Y. Jouan, M. Richard-Plouet, V. Brien, D. Gloaguen, and B. Girault. Flow stress improvement of a nickel multicrystal by physical vapor thin film deposition to reduce surface effects. *Materials Letters : X*, 14 :100145, 2022.